ChemComm

COMMUNICATION

View Article Online
View Journal

Cite this: DOI: 10.1039/c9cc04434e

Received 10th June 2019,
Accepted 8th July 2019

DOI: 10.1039/c9cc04434e

rsc.li/chemcomm

Record-high thermal stability achieved in a novel single-component all-organic ferroelectric crystal exhibiting polymorphism†

Sanjay Dutta,[a] Vikas,[a] Ashok Yadav,[b] Ramamoorthy Boomishankar,[b] Anu Bala,[c] Vijay Kumar,[cd] Tirthankar Chakraborty,[e] Suja Elizabeth[e] and Parthapratim Munshi*[a]

Traditionally, lead and heavy metal containing inorganic oxides dominate the area of ferroelectricity. Although, recently, lightweight non-toxic organic ferroelectrics have emerged as excellent alternatives, achieving higher temperature up to which the ferroelectric phase can persist has remained a challenge. Moreover, only a few of those are single-component molecular ferroelectrics and were discovered upon revisiting their crystal structures. Here we report a novel phenanthroimidazole derivative, which not only displays notable spontaneous and highly stable remnant polarizations with a low coercive field but also retains its ferroelectric phase up to a record-high temperature of ~521 K. Subsequently, the crystal undergoes phase transition to form non-polar and centrosymmetric polymorphs, the first study of its kind in a single-component ferroelectric crystal. Moreover, the compound exhibits a significantly high thermal stability. Given the excellent figures-of-merit for ferroelectricity, this material is likely to find potential applications in microelectronic devices pertaining to non-volatile memory.

Ferroelectric materials, which are electrically polar and exhibit spontaneous polarization (P_s), experience switching of electric polarization (P) under the influence of an external electric field (E).[1] Traditionally, inorganic oxides containing toxic metals *e.g.* $PbTiO_3$ and PZT have dominated this area and found applications in transistors, capacitors, memory devices, infrared detectors, *etc.*[2] This is mainly due to their high Curie temperatures (T_c), high P_s yet stable remnant polarization (P_r) and low coercive fields (E_c). Polymer ferroelectrics[3] have also been used in sensors and in acoustic devices but they experience a large E_c because of their high molecular weights. Recently, organic ferroelectrics have attracted great attention due to their advantages of being lightweight, design flexibility, solution processability and lowest toxicity.[4] However, the majority of organic ferroelectrics reported to date are multi-component systems – salts,[4f–l] and co-crystals.[4f,g] While salts often contain metals or else display a low T_c,[4i] co-crystals have low thermal stability that limits their applicability.[4f,g] So far, the highest T_c of ~500 K has been reported for a metal containing salt ferroelectric crystal, [Hdabco][ReO_4].[4l] In contrast, to the best of our knowledge, very recently, 3-quinuclidinol was reported as the only single-component organic ferroelectric with a T_c of 400 K.[5a] Additionally, there are seven more reports on the above room temperature (RT) single-component organic ferroelectrics.[4b–e,5a] But the ferroelectricity in all of these has been discovered upon revisiting their crystal structures. Moreover, the T_c remained inaccessible, even for the well-known croconic acid (CA)[4b] and the temperatures up to which the ferroelectricity can persist have been reported to be in the range of 357–400 K only. Accordingly, it is concluded that due to the thermal robustness of the ferroelectric phase the T_c of single-component systems is hidden beyond their thermal stability.[5b] Indubitably, other than observing the T_c above RT, achieving thermal stability much above RT has remained extremely challenging in the case of all-organic molecular crystals. Moreover, the challenges persist in the generation of molecular ferroelectric crystals in one of the 10 polar point groups.[1] Therefore, until now, ferroelectricity in a novel single-component organic crystal has remained unexplored.

Organic ferroelectric systems comprising an enamine unit (–HN–C=N–) are reported to follow the proton tautomerism mechanism (PTM), which enables hopping of the proton and π-bond in tandem leading to the generation of P_s under an

[a] Chemical and Biological Crystallography Laboratory, Department of Chemistry, School of Natural Sciences, Shiv Nadar University, Dadri 201314, UP, India. E-mail: parthapratim.munshi@snu.edu.in
[b] Department of Chemistry, Indian Institute of Science Education and Research, Pune, Dr Homi Bhabha Road, Pune 411008, India
[c] Centre for Informatics, School of Natural Sciences, Shiv Nadar University, Dadri 201314, Uttar Pradesh, India
[d] Dr Vijay Kumar Foundation, 1969 Sector 4, Gurgaon 122001, Haryana, India
[e] Department of Physics, Indian Institute of Science, Bangalore 560012, Karnataka, India

† Electronic supplementary information (ESI) available: Synthesis, NMR, HRMS, crystallization, SCXRD data, crystal structures, energy frameworks, lattice energies, DSC, HSM, PXRD, TGA, dielectric and ferroelectric measurements, polarization calculation, SHG experiment and calculations. CCDC 1895789, 1895791, 1895792, 1895794, 1921678 and 1921679. For ESI and crystallographic data in CIF or other electronic format see DOI: 10.1039/c9cc04434e

external E.[4e] On the other hand, ferroelectricity in many of the inorganic compounds[6] and multicomponent molecular crystals[4k,7] is characterized as displacive type, in which P_s arises due to the displacement of different molecular units or ions in a compound. The other mechanism which the ferroelectrics generally follow is the order–disorder type.[4h]

Recent studies on the above RT ferroelectricity in benzimidazoles (BI)[4d] inspired us to explore similar systems with extended benzene rings with a focus on achieving higher thermal stability. Ferroelectricity in some of the haloimidazoles and their mixed crystals has also been explored using piezoresponse force microscopy.[8] An imidazole ring is a fundamental unit of the amino acid histidine, a biologically active substance histamine, many antifungal drugs and anti-tubercular agents. Naturally, imidazoles are environmentally benign and their extensive applications are attributed to their low cost, high solubility and air stability. Being amphoteric, imidazoles can donate as well as accept protons and form intermolecular resonance assisted hydrogen bonds (RAHB),[9] ═C–N–H···N═C– and –C═N···H–N–C═, which enable polarity switching.[4d]

In the context of material characterization, it is imperative to study polymorphism as the polymorphic forms may display distinct properties.[10] Although polymorphism in organic materials with optoelectronic interests is not uncommon,[11] as per our knowledge, a polymorphic study in a single-component molecular ferroelectric has not been reported in the literature yet.

Here, we report notable ferroelectricity (P_s = 3.0 μC cm^{-2} and P_r = 3.9 μC cm^{-2}) with a low E_c (6.2 kV cm^{-1}) in a novel single-component organic crystal of a phenanthroimidazole derivative (**1**, Scheme S1, ESI†). To the best of our knowledge, this is the most thermally stable (~521 K) all-organic ferroelectric crystal, reported to date. In fact, the E_c achieved in this case is much lower than that of the CA[4b] and BI.[4d] Furthermore, we have performed first-principles calculations that also predict a similar value of P_s (~3.8 μC cm^{-2}) as that obtained from the P–E loop measurement at RT. Additionally, we report two more polymorphic forms of **1**, which crystallize in non-polar and centrosymmetric space groups, respectively, both discovered upon sublimation.

Synthesis[12] (Scheme S1) and chemical characterizations (Fig. S1) of **1** are given in the ESI.† Crystallizations (Table S1, ESI†) *via* slow solvent evaporation of **1** resulted in crystals (Fig. S2a, ESI†) of the tetragonal system with a polar space group $P4_1$ (point group 4, hereafter called **1P**) and that contains two crystallographically independent molecules (A and B, Fig. S3a, ESI†) in the asymmetric unit (Z' = 2). Whereas, upon vacuum sublimation at 10 mbar and 503 K, **1** crystallizes (Fig. S2b, ESI†) in the non-polar space group $P\bar{4}2_1c$ (point group $\bar{4}2m$, hereafter called **1N**) with Z′ = 1 (Fig. S3b, ESI†), also in the tetragonal system. Furthermore, during hot-stage microscopy (HSM), upon sublimation, **1P** crystallizes in the monoclinic system with the centrosymmetric space group $P2_1/n$ (point group $2/m$, hereafter called **1C**) with Z' = 2 (Fig. S3c, ESI†).

The details of the single-crystal X-ray diffraction (SCXRD) experiments, crystal data and structural analyses are given in the ESI† (Table S2 and Fig. S3, S4). Here we report the crystal

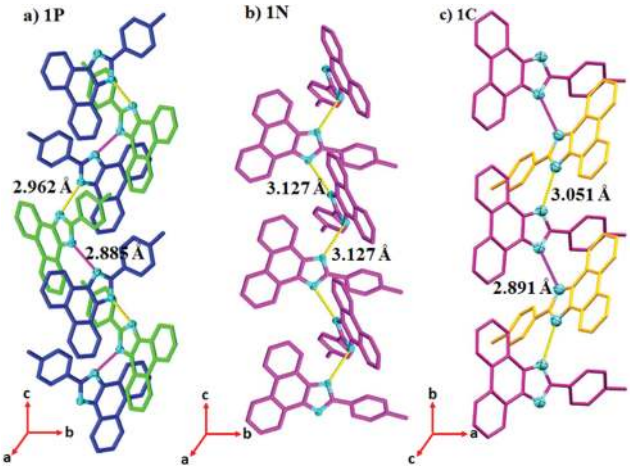

Fig. 1 The capped stick view of (a) discrete N–H···N hydrogen bonds (N_A···H_B = 1.955 Å and N_B···H_A = 2.030 Å) between A (blue) and B (green) molecules in the crystal lattice of **1P**, (b) indiscrete N–H···N hydrogen bonds (N···H = 2.221 Å) in the crystal lattice of **1N** and (c) discrete N–H···N hydrogen bonds (N_A···H_B = 1.955 Å and N_B···H_A = 2.030 Å) between A (blue) and B (green) molecules in the crystal lattice of **1C**. N-atoms in cyan colour are shown as ellipsoids and H-atoms are omitted for clarity.

structures of **1** for the first time. Although we report the variable temperature SCXRD data for **1P**, we focus our discussions based on RT data only. The molecules in the crystal lattice of **1P** adopt ABAB type packing leading to a helical structure (Fig. S5, ESI†) *via* discrete N–H···N hydrogen bonds with N_A···N_B and N_B···N_A distances of 2.885 Å and 2.962 Å, respectively, along the *c*-axis (Fig. 1a). Similar discrete hydrogen bonds have been noticed in the case of ferroelectric MBI (CCDC ref code: KOWYEA). Conversely, **1N** consists of an indiscrete weak N–H···N hydrogen bond with the N···N distance of 3.127 Å, also along the *c*-axis (Fig. 1b) and adopts a butterfly like structure (Fig. S4b, ESI†). For **1C**, the molecules in the crystal lattice also adopt ABAB type packing *via* discrete N–H···N hydrogen bonds as observed in **1P** but along the *b*-axis and with N_A···N_B and N_B···N_A distances of 2.891 Å and 3.051 Å, respectively (Fig. 1c). However, **1C** forms a similar butterfly like structure as **1N** (Fig. S4c, ESI†). The qualitative differences in intermolecular interaction patterns in **1P**, **1N** and **1C** are highlighted in terms of the "energy frameworks"[13] constructed based on the interaction energies (Table S3 and Fig. S5–S7, details in the ESI†). Lattice energy calculations using PIXEL[14] (details in ESI†) suggest that although these three forms have similar energies, the centrosymmetric form **1C** is energetically the most stable form and that of the non-polar form **1N** is the least (Table S4, ESI†).

The thermogram recorded using differential scanning calorimetry (DSC) on the crystals of **1P** (phase I) shows an endothermic peak at ~521 K and transforms to another phase (phase II), which melts at ~563 K (Fig. 2a, bottom plot). However, no crystallization peak is observed during the cooling cycle. The DSC recorded on the crystals of **1N** shows the melting point also at ~563 K (Fig. 2a, top plot). Furthermore, the second heating cycles as plotted in Fig. 2b for both **1P** (bottom plot) and **1N** (top plot) show similar melting points at ~559 K.

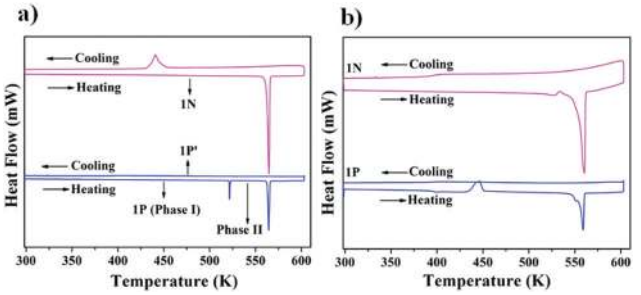

Fig. 2 DSC plots recorded on **1P** (bottom plot in blue solid line) and **1N** (top plot in pink solid line) crystals during (a) the first and (b) the second cycles of heating and cooling. **1P′** is the recovered sample after the first cycle of DSC of **1P**.

Additionally, an exothermic peak appears at ~440 K for each of **1N** (Fig. 2a, top plot) and **1P** (Fig. 2b, bottom plot) during the 1st cooling and 2nd heating cycles, respectively. These broad small peaks signify the partial conversion of the amorphous solids into crystalline solids. The HSM on the **1P** and **1N** crystals displays similar thermal behaviour as observed in Fig. 2a. However, for both, the material partly becomes amorphous upon cooling the melt and crystalline upon sublimation (Fig. S8a, ESI†). Powder X-ray diffraction (PXRD) of the amorphous materials and the SCXRD of the crystals confirm that the resultant materials are in the **1N** form. Nevertheless, for **1P**, although the majority of the crystals are rod-shaped (Fig. S8a at 423 K or 308 K, ESI†) and provide cell-parameters of **1N**, a very few thin needle-like crystals lead to the third polymorph, **1C**, as discussed above. However, due to the insufficient amount of this minor phase (not traceable in DSC) here we study only the crystal structure of **1C**. Furthermore, the PXRD pattern recorded upon crushing the solid sample (**1P′**), recovered after the first heating and cooling cycle in DSC (Fig. 2a), matches exactly with that of **1N** (Fig. S9a, ESI†) and it differs significantly from the PXRD of **1P** (Fig. S9b, ESI†). PXRD of **1P′** was found to match exactly with that of phase II (Fig. 2a), a sample of which was recovered after the 1st cycle of heating of **1P** up to 550 K, in a separate DSC experiment (Fig. S8b, ESI†). Therefore, it is concluded that **1P′** and so the phase II are of non-polar form **1N**. Corroborating these results from DSC, HSM and PXRD (details in ESI†) we infer that the polar form **1P** persists up to a very high temperature (HT) of 521.2 K, after which it transforms irreversibly into the non-polar form **1N** and also to the centrosymmetric form **1C**. Whereas, **1N** retains its phase upon heating and cooling. However, similar to the other single-component molecular ferroelectric crystals, the T_c and hence the paraelectric phase of **1P** also remain hidden due to the thermal robustness of its ferroelectric phase.[5b] Distinct experimental PXRD patterns of **1P** and **1N** (Fig. S9, ESI†) and their exact match with the corresponding simulated PXRD patterns (Fig. S9c and S9d, ESI†) confirm the purity of the respective phases. Furthermore, thermogravimetric analysis (TGA, details in the ESI†) confirms that the thermal decomposition temperature of the **1P** crystal is as high as 658.2 K whereas that of the **1N** crystal is 675.2 K (Fig. S10, ESI†).

Temperature-dependent dielectric measurements along the polar *c*-axis of the **1P** crystal display slow increment of the dielectric constant (ε') with an anomalous behaviour near 515–521 K at 100–20 KHz (Fig. S11a, ESI†). Furthermore, the low dielectric loss in **1P** indicates its insulating nature until the phase transformation temperature (Fig. S11b, ESI†), after which the dielectric loss increases sharply. This is due to the loss of crystallinity of **1P** at HT as observed from the HSM (Fig. S8a at 533 K, ESI†). However, the crystal structure of **1P** is conveniently determined up to 473 K and refined with reasonable reliability factors (Table S2, ESI†).

Ultimately, the evidence of ferroelectricity in **1** is established through *P–E* hysteresis loop measurements at RT along the *c*-axis of the **1P** crystal. At 1 Hz and 600 V, **1P** displays a typical rectangular loop[4d,m] with P_r and P_s values of 3.9 μC cm^{-2} and 3.0 μC cm^{-2}, respectively and E_c of 6.2 kV cm^{-1} (Fig. 3). In our present single-component all-organic molecular crystal containing an enamine unit, while the polarization values are notable the E_c value is much lower than that of BI[4d] and CA.[4b] For the two PTM-type ferroelectrics, BI[4d] forms butterfly like structures *via* linear N–H···N hydrogen bonds, whereas **1P** forms a helical structure with comparable N···N distances (2.9235 Å on an average) and experiences displacive molecular motion within the A···B···A trimeric unit (Fig. 1b), leading to polarization switching under a low E_c. Furthermore, fatigue measurements on **1P** demonstrate that 98% of its P_r along with the rectangle hysteresis loop is retained even after 10^6 switching operation cycles as shown in the remnant polarization loop (Fig. 3, top blue and bottom red curves). Reasonably low leakage currents along with peaks associated with domain switching at 600 V are shown in Fig. S12 (ESI†). Measurements of the *P–E* loop at HT did not show any significant changes in their characteristics in comparison with those obtained at RT. Nevertheless, in this case, a very low value of E_c is achieved at RT.

Moreover, first-principles calculations indicate negligible variation in P_s with temperature (Tables S5–S7, details in the ESI†). The P_s value (~3.8 μC cm^{-2}) estimated from these calculations agrees well with that obtained from the *P–E* loop measurement (3.0 μC cm^{-2}) at RT. A similar increment of ~27%

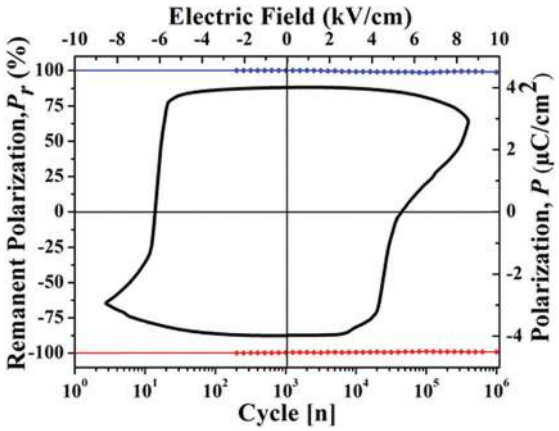

Fig. 3 The rectangular *P–E* hysteresis loop of the **1P** crystal and the corresponding fatigue characteristics for 10^6 switching cycles. The P_r data points in blue (top) and red (bottom) are recorded in forward and reverse bias, respectively.

from the experimental P_s to the theoretical estimation is noticed in the case of CA as well.[4b] Additionally, the calculation at 0 K based on the optimized geometry of **1P**, starting with the 100 K crystal geometry and upon complete relaxation of the cell parameters, resulted in a P_s value of 3.3 μC cm^{-2}. For these calculations, the protons of the N–H groups are shifted from their ordered (ferroelectric phase, degrees of polar distortion $\lambda = 1$) position (N_A–H_A···N_B and NB–HB···NA) to the disordered (hypothetical *para*-electric phase, $\lambda = 0$) position (NA···HA···NB···HB···NA), as typically followed for PTM-type ferroelectrics.[4e] The quantitative agreement between the experimental and theoretical values of P_s confirms the ferroelectric characteristic of **1**.

Second harmonic generation (SHG) activity measurements on homogeneous powdered samples of both **1P** (polar) and **1N** (non-polar) crystals reveal that **1P** is almost as active as KDP, an inorganic ferroelectric material, giving rise to an SHG signal of 18 mV (Table S8, ESI†). Whereas, as expected, the non-polar **1N** displays a much reduced SHG signal of 5 mV. Furthermore, the estimation of SHG properties based on periodic calculations[11c] using crystal geometry as obtained from the SCXRD experiment at RT suggests similar trends (Table S9, details in ESI†).

In conclusion, here we report phenanthroimidazole derivative, **1**, a novel single-component all-organic crystal, which persists in its ferroelectric phase up to a record-high temperature of ∼521 K. Moreover, the ferroelectric crystal exhibits a significantly high thermal decomposition temperature (∼658 K). Indeed, migrating from benzimidazoles to phenanthroimidazoles with extended benzene rings helped in achieving the ferroelectric phase up to a much higher temperature. Furthermore, we believe that although the generation of polarization and polarity switching is triggered by the PTM *via* RAHB in **1**, the low E_c is achieved due to molecular displacements in its crystal lattice. The notable yet stable polarizations, low E_c and record-high thermal stability make **1** a potent organic ferroelectric material for promising applications in non-volatile memory devices such as FeRAM and memristors. Here we also discover that **1** undergoes polymorphic transitions at high temperatures to form non-polar and centrosymmetric crystal structures – the first study of its kind in a single-component ferroelectric crystal.

SD and Vikas thank Shiv Nadar University (SNU) for research fellowships. This work was supported by SNU and SERB grant to PM (CRG/2018/004694). The calculations are performed using the high performance computing facility at SNU and the computer workstation procured through SERB grant (EMR/2014/000491) to PM. AB thanks DST India for the women scientist fellowship (grant No. SR/WOS-A/PM-1042/2015). RB thanks SERB grant (EMR/2016/000614). We thank Dr Ashish Kundu for useful discussion.

Conflicts of interest

The authors declare no conflict of interest.

References

1 M. E. Lines and A. M. Glass, *Principles and Applications of Ferroelectrics and Related Materials*, Oxford University Press, 2001.
2 (*a*) J. F. Scott, *Ferroeleetrie Memories*, Springer, 2000; (*b*) J. F. Scott, *Science*, 2007, **315**, 954–959.
3 (*a*) T. Furukawa, M. Date and E. Fukada, *J. Appl. Phys.*, 1980, **51**, 1135–1141; (*b*) T. Furukawa, *Phase Transitions*, 1989, **18**, 143–211; (*c*) K. Noda, K. Ishida, A. Kubono, T. Horiuchi, H. Yamada and K. Matsushige, *J. Appl. Phys.*, 2003, **93**, 2866–2870.
4 (*a*) S. Horiuchi and Y. Tokura, *Nat. Mater.*, 2008, **7**, 357–366; (*b*) S. Horiuchi, Y. Tokunaga, G. Giovannetti, S. Picozzi, H. Itoh, R. Shimano, R. Kumai and Y. Tokura, *Nature*, 2010, **463**, 789–792; (*c*) S. Horiuchi, R. Kumai and Y. Tokura, *Adv. Mater.*, 2011, **23**, 2098–2103; (*d*) S. Horiuchi, F. Kagawa, K. Hatahara, K. Kobayashi, R. Kumai, Y. Murakami and Y. Tokura, *Nat. Commun.*, 2012, **3**, 1308; (*e*) S. Horiuchi, K. Kobayashi, R. Kumai and S. Ishibashi, *Nat. Commun.*, 2017, **8**, 14426; (*f*) A. S. Tayi, A. Kaeser, M. Matsumoto, T. Aida and S. I. Stupp, *Nat. Chem.*, 2015, **7**, 281–294; (*g*) R. A. Wiscons, N. R. Goud, J. T. Damron and A. J. Matzger, *Angew. Chem., Int. Ed.*, 2018, **57**, 9044–9047; (*h*) P. P. Shi, Y. Y. Tang, P. F. Li, W. Q. Liao, Z. X. Wang, Q. Ye and R. G. Xiong, *Chem. Soc. Rev.*, 2016, **45**, 3811–3827; (*i*) Z. S. Yao, K. Yamamoto, H. L. Cai, K. Takahashi and O. Sato, *J. Am. Chem. Soc.*, 2016, **138**, 12005–12008; (*j*) T. Vijayakanth, A. K. Srivastava, F. Ram, P. Kulkarni, K. Shanmuganathan, B. Praveenkumar and R. Boomishankar, *Angew. Chem., Int. Ed.*, 2018, **57**, 9054–9058; (*k*) H.-Y. Ye, Y.-Y. Tang, P.-F. Li, W.-Q. Liao, J.-X. Gao, X.-N. Hua, H. Cai, P.-P. Shi, Y.-M. You and R.-G. Xiong, *Science*, 2018, **361**, 151–155; (*l*) Y. Y. Tang, P. F. Li, W. Y. Zhang, H. Y. Ye, Y. M. You and R. G. Xiong, *J. Am. Chem. Soc.*, 2017, **139**, 13903–13908; (*m*) H. Ma, W. Gao, J. Wang, T. Wu, G. Yuan, J. Liu and Z. Liu, *Adv. Electron. Mater.*, 2016, **2**, 1600038; (*n*) W.-Q. Liao, D. Zhao, Y.-Y. Tang, Y. Zhang, P.-F. Li, P.-P. Shi, X.-G. Chen, Y.-M. You and R.-G. Xiong, *Science*, 2019, **363**, 1206–1210; (*o*) C. Yang, W. Chen, Y. Ding, J. Wang, Y. Rao, W. Liao, Y. Tang, P. Li, Z. Wang and R. Xiong, *Adv. Mater.*, 2019, **31**, 1808088; (*p*) Y. Ai, X.-G. Chen, P.-P. Shi, Y.-Y. Tang, P.-F. Li, W.-Q. Liao and R.-G. Xiong, *J. Am. Chem. Soc.*, 2019, **141**, 4474–4479.
5 (*a*) P.-F. Li, W.-Q. Liao, Y.-Y. Tang, W. Qiao, D. Zhao, Y. Ai, Y.-F. Yao and R.-G. Xiong, *Proc. Natl. Acad. Sci. U. S. A.*, 2019, **116**, 5878–5885; (*b*) S. Horiuchi, R. Kumai and S. Ishibashi, *Chem. Sci.*, 2018, **9**, 425–432.
6 (*a*) B. T. Matthias and J. P. Remeika, *Phys. Rev. Lett.*, 1947, **76**, 1886; (*b*) R. S. Weis and T. K. Gaylord, *Appl. Phys. A: Solids Surf.*, 1985, **37**, 191–203; (*c*) G. H. Kwei, A. C. Lawson, S. J. L. Billinge and S. W. Cheong, *J. Phys. Chem.*, 1993, **97**, 2368–2377.
7 (*a*) H.-L. Cai, W. Zhang, J.-Z. Ge, Y. Zhang, K. Awaga, T. Nakamura and R.-G. Xiong, *Phys. Rev. Lett.*, 2011, **107**, 147601; (*b*) Z. Sun, T. Chen, J. Luo and M. Hong, *Angew. Chem., Int. Ed.*, 2012, **51**, 3871–3876; (*c*) M. Szafrański, *Angew. Chem., Int. Ed.*, 2013, **52**, 7076–7078; (*d*) H. Y. Ye, Y. Zhang, D. W. Fu and R. G. Xiong, *Angew. Chem., Int. Ed.*, 2014, **53**, 6724–6728.
8 M. Owczarek, K. A. Hujsak, D. P. Ferris, A. Prokofjevs, I. Majerz, P. Szklarz, H. Zhang, A. A. Sarjeant, C. L. Stern, R. Jakubas, S. Hong, V. P. Dravid and J. F. Stoddart, *Nat. Commun.*, 2016, **7**, 13108.
9 G. Gilli, F. Bellucci, V. Ferretti and V. Bertolasi, *J. Am. Chem. Soc.*, 1989, **111**, 1023–1028.
10 W. C. McCrone, *Physics and chemistry of the organic solid state*, ed. D. Fox, M. M. Labes and A. Weissberger, Wiley Interscience, New York, USA, 1965, vol. 2.
11 (*a*) K. Kobayashi, S. Horiuchi, S. Ishibashi, F. Kagawa, Y. Murakami and R. Kumai, *Chem. – Eur. J.*, 2014, **20**, 17515–17522; (*b*) H. Chung and Y. Diao, *J. Mater. Chem. C*, 2016, **4**, 3915–3933; (*c*) K. K. Jha, S. Dutta and P. Munshi, *Cryst. Growth Des.*, 2018, **18**, 1126–1135.
12 W. Lin, L. Long, L. Yuan, Z. Cao, B. Chen and W. Tan, *Org. Lett.*, 2008, **10**, 5577–5580.
13 M. J. Turner, S. P. Thomas, M. W. Shi, D. Jayatilaka and M. A. Spackman, *Chem. Commun.*, 2015, **51**, 3735–3738.
14 A. Gavezzotti, *Z. Kristallogr.*, 2005, **220**, 499.

